Exploring Topological Defects in Epitaxial $BiFeO_3$ Thin Films

Rama K. Vasudevan,[†] Yi-Chun Chen,[‡] Hsiang-Hua Tai,[‡] Nina Balke,[§] Pingping Wu,[⊥] Saswata Bhattacharya,[⊥] L. Q. Chen,[⊥] Ying-Hao Chu,[¶] I-Nan Lin,[#] Sergei V. Kalinin,*[,§] and Valanoor Nagarajan[†,*]

[†]School of Materials Science and Engineering, University of New South Wales, Sydney 2052, Australia, [‡]Department of Physics, National Cheng Kung University, No.1, University Road, Tainan City 701, Taiwan R.O.C., [§]The Center for Nanophase Materials Sciences, Oak Ridge National Laboratory, Oak Ridge, Tennessee 37831, United States, [⊥]Department of Materials Science and Engineering, Penn State University, University Park, Pennsylvania 16802, United States , [¶]Department of Materials Science and Engineering, National Chiao Tung University, Hsinchu 30010, Taiwan, and [#]Department of Physics, Tamkang University, Tamsui 251, Taiwan

ABSTRACT Using a combination of piezoresponse force microscopy (PFM) and phase-field modeling, we demonstrate ubiquitous formation of center-type and possible ferroelectric closure domain arrangements during polarization switching near the ferroelastic domain walls in (100) oriented rhombohedral $BiFeO_3$. The formation of these topological defects is determined from the vertical and lateral PFM data and confirmed from the reversible changes in surface topography. These observations provide insight into the mechanisms of tip-induced ferroelastic domain control and suggest that formation of topological defect states under the action of local defect- and tip-induced fields is much more common than previously believed.

KEYWORDS: $BiFeO_3$ · closure-domain · topological defects · multiferroic · thin-film · PFM

The key aspect of materials that exhibit long-range order is the presence of topological defects in the order parameter field, ranging from dislocations and disclinations in liquid crystals and crystalline solids,[1] to domain walls in ferroics[2] to exotic defects in superconductors and charge-density wave materials. Materials functionality in virtually all dynamic processes is determined by the types and mobility of these topological defects and their interactions with structural elements such as point defects, dislocations, surfaces, and interfaces. In ferroic systems with a vector order parameter, the detailed classification was given by Mermin, and includes a variety of 2D and 1D extended defects.[3] The well-known 2D topological defects include domain walls, the dynamics of which underpins virtually all aspects of ferroelectric behavior ranging from nonlinear piezoelectric responses to ferroelectric polarization switching.[4] However, 1D defects, including vortex and antivortex states (corresponding to "winding numbers" $n = +1$, $n = -1$, respectively, in Mermin's definition), have remained elusive until very recently,[5] owing to the difficulties of experimental observations.

In ferroelectrics, the formation of a vortex-type defect lowers the depolarization energy (all domains are head to tail), but increases strain energy due to linear piezoelectric coupling between the order parameter and lattice strain. In ferromagnets, the coupling between magnetization and lattice strain is weak (10^{-6}–10^{-4}),[6] and the magnetization cannot be screened (due to the lack of magnetic monopoles), favoring the formation of vortex states. The first observation of magnetic vortex states was reported in 1980 in a 55 nm-thick Co film,[7] although studies of in-plane domain orientations date back further considerably.[8] Subsequently, extensive modeling has demonstrated that formation of vortex states is a ubiquitous aspect of a magnetization switching process in nanostructures.[9−11] Topological defect states have also been found to be present in ferroelectromagnetic materials, such as $YMnO_3$.[12−14] Compared with magnetic systems, in ferroelectrics the strains are much higher (10^{-3}–10^{-2}),[15] thus resulting in much higher strain energy penalty of the vortex state. Following the initial work of Gorbatsevich and Kopaev,[16] the interest in these systems remained dormant until recent first-principles studies by Naumov *et al.*,[17] and the subsequent explosion of theoretical work in this area.[18−22] Similar to magnetic systems, the formation of the vortex state was postulated to result from the interplay between strain and depolarization energy. The strain energy diverges with the system size (since the vortex core acts as a disclination center) and, hence, vortex formation is expected to be limited to nanoscale systems under conditions of poor polarization screening, setting the background to experimental activity in the area. Transient vortex states have been inferred by Gruverman *et al.* to exist in circular PZT capacitors upon switching.[23] Practically however, observation of vortex states is limited

*Address correspondence to sergei2@ornl.gov, nagarajan@unsw.edu.au.

Received for review May 18, 2010 and accepted December 24, 2010

Published online January 07, 2011
10.1021/nn102099z

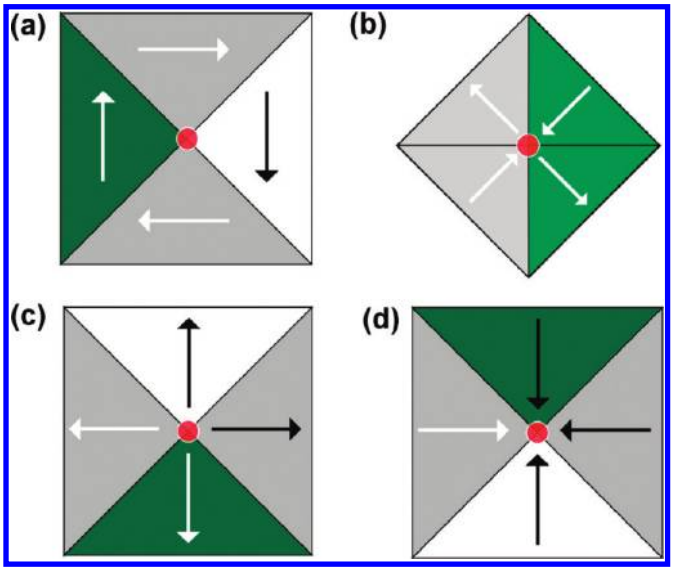

Figure 1. Schematics of possible topological defects formed upon switching. Schematic a shows a vortex state, while schematic b shows an antivortex (analogous to ferromagnetic vortices). The rosette structures (center-type domains) depicted in panels c and d couple effectively with the in-plane components of the tip-field. In these cases, the tip-field favors formation of a domain junction between two charged domain walls, with schematic c expected for a positive tip−sample bias, and schematic d expected for opposite bias. There exists a disclination center at the topological defect core (red circles) indicated by a topographical feature (an elevation or depression), discussed further in Figure 6.

by finite resolution. For example, piezoresponse force microscopy (PFM) studies of arrays of tetragonal PZT nanodots by Rodriguez *et al*. appear to indicate the formation of complex closure domain states resembling simulated vortex states.[24] Schilling *et al.* have shown the formation of vortex-like closure domains within near single-crystal $BaTiO_3$ nanodots.[25] Recently, McGilly *et al.* have found chains of interlinking flux-closure domains and quadrupole states occurring naturally in single crystal $BaTiO_3$ lamellae.[26] In their studies, it was determined that the domain quadrants arrange themselves with an additional 180° wall so as to avoid the formation of a disclination center. The controlled formation of the vortex−antivortex closure domain lines in continuous films was demonstrated by Balke *et al*.[27] However, thus far such states have not been found to form spontaneously underneath a proximal probe.

The driving force for topological defect formation is the electric field produced by the external bias applied to the scanning probe microscope (SPM) tip (which we define as the "tip-field"). In this paper, we demonstrate that, through careful selection of domain crystallography and electrical boundary conditions, it becomes possible to spontaneously form topological defects underneath a biased SPM tip.

For all cases of materials symmetry, formation of the vortex state by the SPM tip-field is a nontrivial process. The formation of a vortex directly under the tip is highly unlikely in the normal ferroelectric, as the in-plane polarization components of the vortex state do not couple with the in-plane components of the tip-field. However, in the presence of structural defects or topological defects, the inherent radial symmetry of the tip-field is broken, subsequently allowing formation of vortex-type topological defects (for more details of this symmetry breaking, see ref 27). Indeed, the breaking of symmetry by impurities to yield complex domain structures has also been found in other systems.[28] The different types of topological defects that can be created by polarization switching in the film are shown in Figure 1. Two classical arrangements are shown in Figure 1a and 1b, representing a "pure" vortex state and an antivortex, respectively. Vortices have been reported more commonly in the literature. In contrast, a much less-documented class of defect can also be formed, wherein applying an external bias to the tip induces the formation of a domain that effectively couples to the tip-field and maintains radial symmetry (albeit lowered due to crystallographic anisotropy effects). In this case, the in-plane components of the tip-field favor the formation of head-to-head (or tail-to-tail) arrangements. These have been defined as so-called center domains by Mermin and are illustrated in Figure 1c,d. Since the center domains contain charged domain walls, they require efficient bulk screening for stabilization.

In the literature, the formation of topological defects such as antivortices and center domains have attracted significantly less attention, despite the rich physics associated with such states. For instance, centers corresponding to converging polarization vectors are expected to have elastically strained cores and charged domain walls, suggesting their intrinsic instability. Until recently, the creation of nonvortex topological defects by a biased SPM tip, have not been actively pursued.

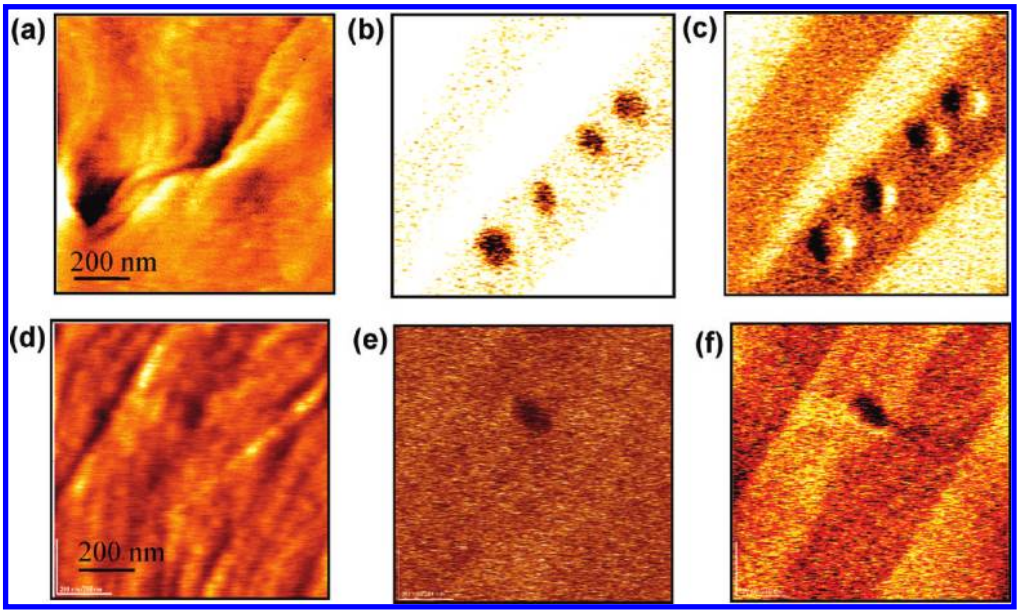

Figure 2. Topography (a,d), out-of-plane PFM scans (b,e) and in-plane PFM scans (c,f) of the film after bias has been applied. In-plane PFM scans of the film after application of four separate pulses away from the domain wall (the case shown in panel c and one pulse at the wall (the case shown in panel f) illustrate the crucial role of the interface in determining the resulting domain structure. In both image sets, −15 V/1 s pulses were applied.

Here, we demonstrate the formation of topological defects, including center-type domain arrangements and possible closure domains, during switching in rhombohedral $BiFeO_3$ by the biased SPM tip. We note that unlike the case for Balke *et al.*,[27] the domains reported here are spontaneously formed by the localized tip-field without local manipulation by proximal probe motion. We adopt Mermin's definition for topological defects, which stipulates that a defect is a site (points, lines, or surfaces) at which the order parameter in the nonuniform media ceases to vary continuously, forming singular regions of lower dimensionality. The presence of ferroelastic domain walls allows symmetry breaking of the radially invariant tip-field, permitting formation of complex domain arrangements. The center-type defects form naturally due to the polarization alignment under strong localized tip-fields, and are stabilized by clamping effects and possibly polarization compensation by charge carriers in $BiFeO_3$. Subsequent visualization of polarization distribution by the PFM illustrates the formation of the topological defects, as further confirmed by phase-field modeling. Finally, we demonstrate the reversible changes in surface topography, indicative of the presence of disclinations at the topological defect cores.

RESULTS AND DISCUSSION

Experimental Observations. As a model system, we have chosen rhombohedral $BiFeO_3$ (BFO) in the (001) orientation grown on (100) $SrRuO_3$-buffered (SRO) $DyScO_3$ (DSO) substrates. The BFO films have a thickness of 800 nm, and were grown on a 40 nm-thick SRO buffer (electrode) on high quality single-crystal (110) DSO substrates. Such a configuration results in formation of equal-width stripe domains with walls parallel to {011} (see Supporting Information, Figure S1). Previous experimental data showed our ability to engineer stripe ferroelastic domains with optimal spacing (200 nm) by controlling anisotropic strains using DSO substrates and growth conditions.[29] This allows single-domain walls to be manipulated and perturbed, without collective interactions.[30,31] In the BFO studied here, the presence of in-plane polarization inhomogeneities (71° domain walls) allows breaking of the tip-field's radial symmetry and, hence, establishes the conditions for formation of other topological defect configurations. Note that this material has two equivalent upward-oriented polarization states, (*hk*1), and equivalent downward-oriented polarization states, (*hk*−1), where $h, k = \pm 1$.

The requirement of a pre-existing defect structure in order to break the symmetry of the tip-field and form more complex domain patterns is shown in Figure 2. Accordingly, this figure shows the results of tip-field induced polarization switching both away from, and at, the domain wall. The topography and domain pattern evolution is shown in Figure 2a−c for the case of a negative tip bias, with the tip located far from the domain wall, for four separate pulses of −15 V (pulse width 1 s). The topography scan is displayed in Figure 2a. The dark contrasts in the out-of-plane image (OP-PFM) shown in Figure 2b indicates uniform polarization switching in the vertical components where the tip was placed, while the in-plane image (IP-PFM) shown in Figure 2c displays two contrasts, indicating two distinct in-plane directions. This proves that both

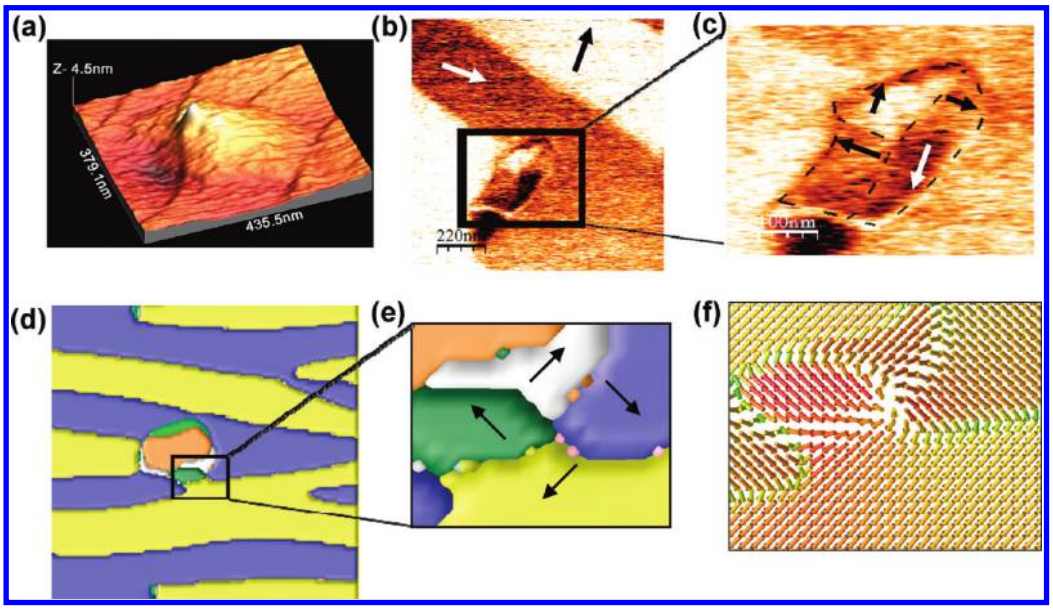

Figure 3. Close-up topography (a), IP-PFM image (b), and close-up IP-PFM image (c) of a domain pattern formed by application of −20 V, 20 s tip−sample bias at the domain wall. Arrows in the IP-PFM image indicate a possible assignment of polarization directions. In the set of images a−c we have observed a multidomain junction. The domains comprising this domain junction are clearly outlined by the dashed line in the close-up in panel c. Phase-field modeling of a closure domain pattern is shown in panels d−f, with the top-down view of the domain state (d), the close-up of the boxed region in panel d (e), and the associated polarization map (f).

vertical and lateral components are undergoing switching as a result of the tip field, but note that the polarization switching is straightforward and does not result in formation of exotic defect states. However, when the tip is placed at the domain wall (Figure 2d−f), the result differs significantly, with a more complex domain structure and significant domain wall rotation observed. Thus, these ferroelastic domain walls are the key to breaking the tip-field's radial symmetry, facilitating formation of more complex states.

When pulses of large amplitude are applied at the wall, we eventually observe formation of topological defects. Theoretically, application of a large bias at the interface (*ca.* −30 V) can result in the formation of complete closure domains (a vortex-like state), or a junction between two oppositely charged domain walls (referred to as the antivortex-like state). We show experimentally in Figure 3 the domain pattern resulting from application of a high voltage pulse at the wall, with the topography around the switched area in Figure 3a, the IP-PFM image in Figure 3b and a close-up of the IP-PFM in Figure 3c. In Figure 3c, there appears clear formation of a multidomain junction. The choice of assignment of polarization directions depicted in Figure 3c is such that it is energetically most favorable; it appears that a closure domain pattern has formed. The significant relaxation of the structure precluded an orthogonal scan to confirm these direction assignments. Extensive details of assignment of the polarization directions are given in Supporting Information, Figure S2. Comparing the schematics in Figure 1, we can see that if Figure 3c does indeed contain the same in-plane polarization directions as in Figure 1a, then this domain arrangement will be expected to have a similar disclination center. To further explore the domain structures that were observed, phase-field modeling was undertaken.

Phase-Field Modeling. The ferroelectric domain structure on the epitaxial BFO thin film was modeled using the phase-field method,[32] in which the spontaneous polarization distribution, and thus the domain structure and its evolution, is governed by the time-dependent Ginzburg−Landau (TDGL) equations.[33] Details of the simulation method can be found in our previous publications.[34−36] To obtain a two-domain structure, we started from a paraelectric state with zero polarization plus small polarization perturbations along the $[1\bar{1}\bar{1}]$ and $[\bar{1}\bar{1}\bar{1}]$ directions and annealed the system at room temperature. The virgin two-domain structure can be seen in Supporting Information, Figure S3. It consists of blue $[1\bar{1}\bar{1}]$ domains and yellow $[\bar{1}\bar{1}\bar{1}]$ domains, separated by 71° domain walls parallel to the (011) plane, approximately 45° from the interface between the thin film and the substrate.

To simulate the PFM tip on the surface of the thin film in the phase-field method, we assumed the following electrical potential distribution,

$$\phi_{\text{appl}} = \phi_{\text{a}} \frac{r_0}{\sqrt{(x_1 - x_0)^2 + (x_2 - y_0)^2 + r_0^2}} \quad (1)$$

where ϕ_a is the voltage applied on the surface of thin film with the conductive tip, (x_0,y_0) is the tip location, and r_0 is the effective radius, and x_1, x_2 are the

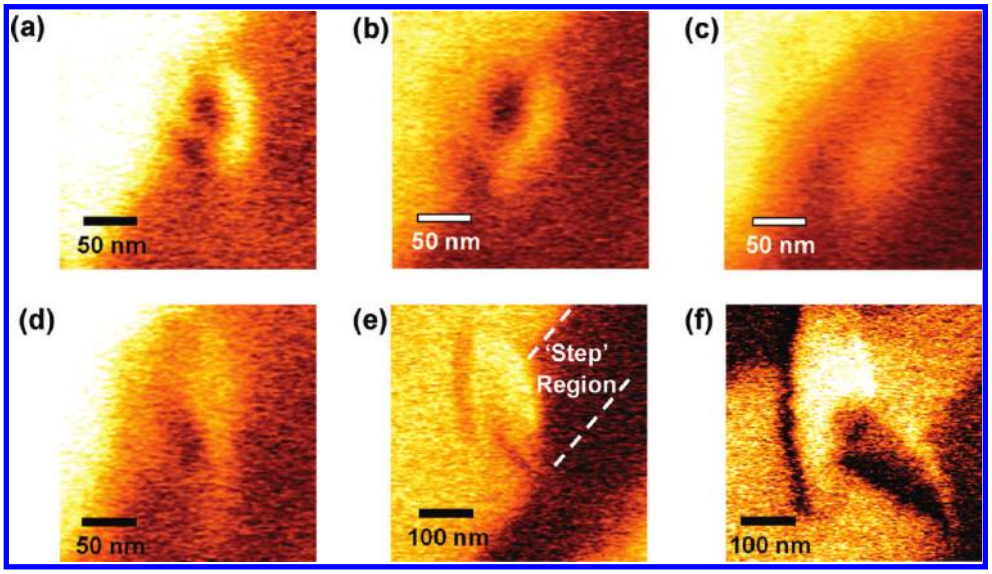

Figure 4. (a−f) IP-PFM images taken after application of negative bias at the domain wall with increasing voltage. The biases used were −16, −18, −20, −24, −26, and −30 V, respectively. With increasing bias, the degree of domain wall rotation increases. The region defined by the existing domain wall growing perpendicularly in a lateral direction is termed the "step" region, as shown in panel e. (f) At −30 V the domain twist is large enough to produce a highly complex domain structure spanning the as-grown stripe domains.

coordinates on the surface. The electric potential on the bottom surface of film is kept at zero.

Figure 3d shows a simulation of a closure domain state in the BFO film. The close-up is shown in Figure 3e with the corresponding polarization distribution map in Figure 3f. There appears close agreement between the phase-field model in Figure 3f and the experimental closure domain pattern seen in Figure 3c. The domain state was modeled by assuming a four-domain random noise distribution in a region between the virgin two domain structure, allowing the system to reach a metastable state, and subsequently approaching the center of the metastable domain with a PFM tip biased at +6 V. It is noteworthy that the phase field model in Figure 3e appears to show a small, extra wall at the center (between the green and blue domains). This type of extra, elongated wall was also observed by McGilly *et al*. in flux-closure domains found in $BaTiO_3$ lamellae, and will presumably form to prevent disclinations that would otherwise arise from a true four-domain junction.[26] Experimentally, determining whether this is indeed the case is limited by the resolution of the PFM system employed.

Formation and Stability of Topological Defect States. Experimentally, we have found that the closure domain state relaxes quickly; hence, exploring the dynamics of formation of these states is considerably more difficult. The inherently limited time resolution (at lowest quality, each scan takes at least 128 s to capture with our experimental setup) of the PFM image capture techniques used here generally prohibits classical polarization relaxation experiments (as breakdown may be on the order of a few seconds), so instead this must be undertaken in a quasi-dynamic fashion. A simple experiment that provides insight into the formation of some of the complex domain arrangements observed is shown in Figure 4. Here, 1 s pulses of varying amplitudes were applied through the tip at the domain wall, with the resulting domain structures imaged (IP-PFM images are shown). At low voltages (Figure 4a,b) there is a slight domain wall twist, accompanied by a small "step" region. With increasing voltage (Figure 4c−e), however, the degree of rotation increases significantly, along with the size of the step, until finally the driving force is sufficiently large to form a complex pattern spanning the two stripe domains (Figure 4f, see Supporting Information, Figure S5 for polarization direction analysis). At lower voltages, such states are unlikely to form, due to the requirement of switching multiple in-plane polarization directions (an inherently nontrivial process).

In addition, it has been predicted by Balke *et al*.[27] and demonstrated in PZT by Varatharajan *et al*.[37] that nucleation bias for domains is significantly reduced at domain walls, as a result of domain wall twist; in this experiment, we have validated that the macroscopic twist indeed occurs. Indeed, it appears that such rotations are crucial for formation of exotic states.[31]

Interestingly, the phase-field models predict that upon application of larger electric fields, the type of the topological defect shows a drastic change, namely the formation of center-type domains. Figure 5a and 5b show simulations of two center-type domain structures on the BFO thin film; the tip location is at the center of the thin film, exactly at the 71° domain wall of the two-domain structure. In the first simulation, displayed in Figure 5a, the applied voltage is $\phi_a \approx -40$ V, and $r_0 = 10$ nm. The ferroelectric domains along the

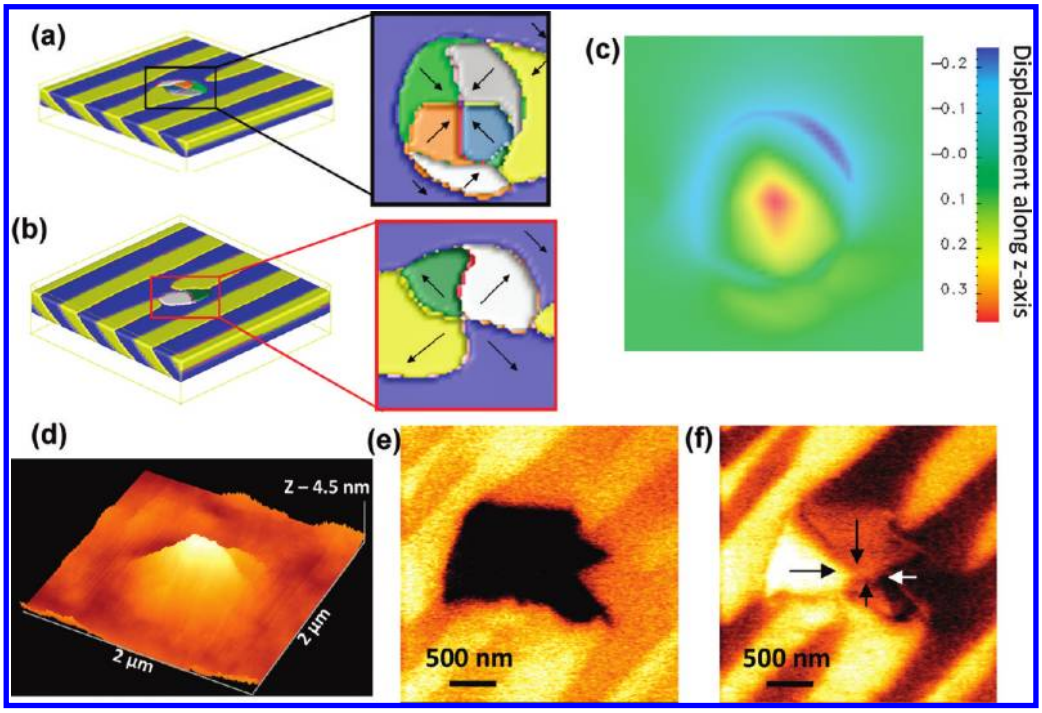

Figure 5. Phase-field modeling (a−c) of a center-type domain arrangement and experimental data (d−f). (a) The phase-field simulation shows a center-type domain arrangement, with polarization vectors pointed toward the center, drawn in the inset. (b) The phase-field simulation shows an alternative center-type arrangement, with vectors pointing away from the core, and is as predicted for the opposite tip bias. (c) Simulated displacement map from the center-type domain arrangement depicted in panel a. (d−f), PFM image set with topography (d), OP-PFM (e), and IP-PFM (f) is shown for a domain produced by −30 V, 1 s pulse applied through the tip at the domain wall. Arrows in panel f indicate in-plane polarization directions. Note the agreement between the structure in panel f and the phase-field model in panel a, as well as the similarity between the displacement map in panel c and the experimental result in panel d.

pseudocubic [111] (orange), [1$\bar{1}$1] (light green), [$\bar{1}$11] (navy blue), and [$\bar{1}\bar{1}$1] (gray) directions form a center-type domain arrangement, with polarization vectors oriented toward the core, as drawn in the inset in Figure 5a. The displacement map predicted by this center-type domain arrangement is shown in Figure 5c. In the second simulation displayed in Figure 5b, the applied voltage $\phi_a \approx +40$ V, and $r_0 = 10$ nm. In this case, the [11$\bar{1}$] domain (white) and the [$\bar{1}$1$\bar{1}$] domain (dark green) are observed in the simulation, along with the two-domain thin film, forming an alternative center-type domain arrangement. Again, the polarization directions are drawn in the corresponding inset. Experimental demonstration of formation of these defect structures is shown in the topography and PFM images in Figure 5d−f. A center-type domain was produced by applying a relatively high voltage (−30 V, 1 s pulse) through the tip at the domain wall. At lower voltages, we do not observe these states forming. Information on polarization assignment is contained in Supporting Information, Figure S4. The topographical scan around the region of the center-type domain is shown in Figure 5d. There appears to be good agreement between the predicted displacement map in Figure 5c and the experimental results in Figure 5d, with the displacement maximum at the core of the topological defect. Similarly, there appears close agreement between the simulation in Figure 5a, and the experimental result in Figure 5f, suggesting that these are, indeed, center-type domain arrangements forming in the BFO film. One should note that the phase-field simulations (see Supporting Information, Figure S3) show that the center-domain state reaches through-thickness only at high applied fields. This confirms our previously stated argument that center-type domains are energetically more expensive to form.

In contrast to vortices and antivortices, the formation of center-type topological defects preserves the radial symmetry of the tip-field. Such configurations are energetically favorable under the tip-field, as the rosette structures Figure 1(c,d) couple effectively with the in-plane components of the tip-field, reducing electrostatic energy. However, this state requires head-to-head (or tail-to-tail, for opposite tip bias) polarization arrangements at the tip site, resulting in formation of charged domain junctions. Thus, adequate charge screening is a prerequisite for stabilization of these topological defect states. Lastly, due to requirements of switching multiple in-plane components simultaneously, and the intrinsic instability of the center-type domain, we expect formation to require relatively large tip-fields.

The phase-field modeling provides straightforward explanation for the formation of center-type domains due to direct coupling of polarization and electric field

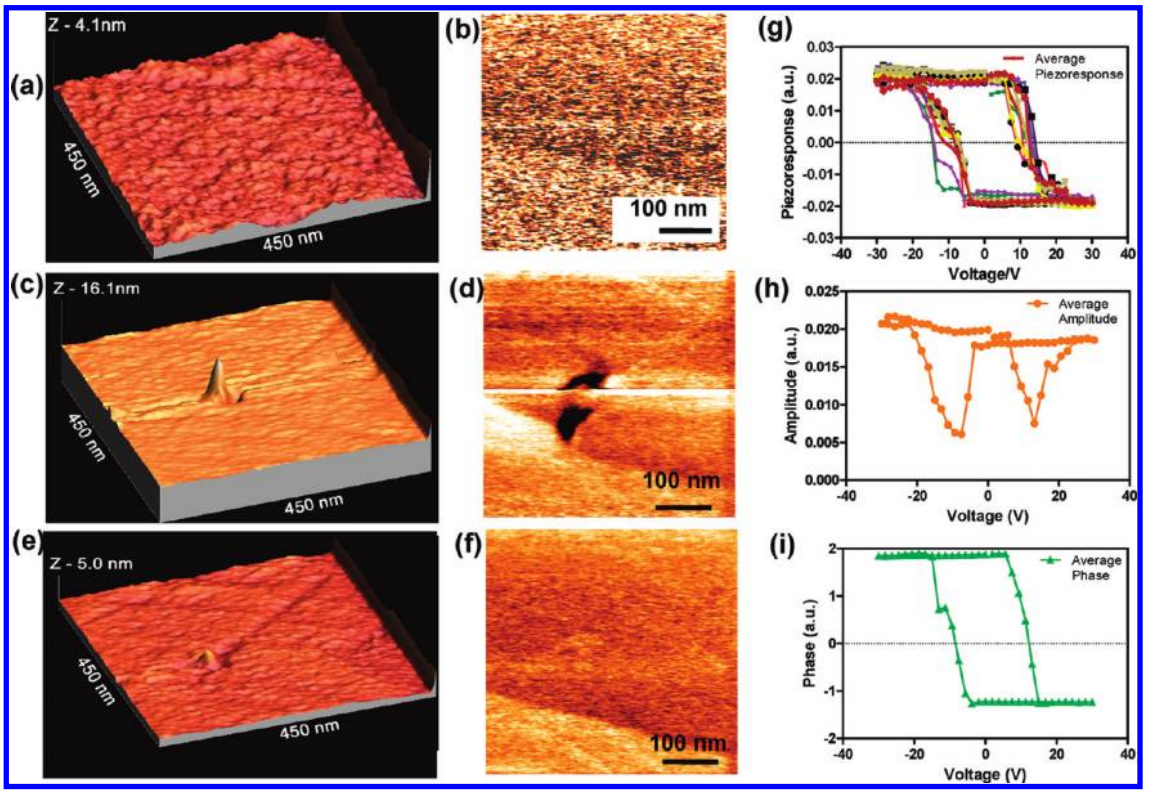

Figure 6. Formation and reversal of topographical feature: (a, c, e) topography is shown with the (b, d, f) corresponding OP-PFM images. A virgin scan is shown in panels a and b. A −12 V bias is then applied at the domain wall, and the result is shown in (c, d). Subsequent application of a two +12 V pulses at the same location yields the (e) topography and (f) OP-PFM image. The domains structure has returned to the virgin state, and the topographical feature has largely disappeared. This reversible change in surface topography is indicative of formation of a disclination at the defect core. (g) Nine hysteresis loops obtained at a single point by the PFM tip in a different region of the sample, at the center of a multidomain junction (voltage ramps from −30 V to +30 V). The average of the nine loops is bold and maroon-colored; (h) associated average amplitude and (i) phase hysteresis loops. These loops suggest that the sample retains ferroelectric properties (and is not damaged) even after repeated application of high voltage pulses through the tip.

of the probe. Somewhat more surprising is that these structures are stable in the field-off state, since they are formed by charged domains walls. We propose that this behavior may be achieved through clamping by surrounding ferroelastic domains, and also compensation of the polarization charges by screening charges and ionic diffusion.

Observation of Disclination on Defect Cores. Notably, independent evidence of formation of the topological defect states is given by the existence of a disclination at the defect core due to elastic mismatch between the domains. The associated change in topography must be reversible and repeatable, to prove that the topographical feature is polarization-dependent and not the result of electro-chemical effects. Shown in Figure 6a,b is a topography and OP-PFM image, respectively, of the film before application of bias. A −12 V pulse is then applied through the tip at the domain wall, with resulting changes in topography and domain structure displayed in Figure 6c,d. Clearly, there appears a large spike-like feature in Figure 6c where the domain has nucleated. When the opposite bias is subsequently applied (+12 V), the topographical spike feature has vanished, as can be seen in Figure 6e, and the domain structure, shown in Figure 6f, largely returns to the virgin state. Note here, however, that the domain structure and topography are not identical to the virgin states, as many factors (such as tip degradation, imprint, local defects) will affect the switching. Finally, to confirm that the film is stable at the high voltages used in these experiments, a multidomain junction was formed by applying a −25 V pulse through the probe. Subsequently, nine switching loops were obtained by ramping through ±30 V at the center of the multidomain junction. The nine loops, and their average, are shown in Figure 6g−i, with piezoresponse in Figure 6g, with corresponding (average) amplitude hysteresis in Figure 6h, and (average) phase hysteresis in Figure 6i. The switching loops vary very little over the cycle, suggesting that the film's ferroelectric properties are unaffected by application of these high voltage pulses. In summary, the reversible change in topography indicates the presence of a disclination at the topological defect core.

SUMMARY

Combining piezoresponse force microscopy and phase-field modeling, we demonstrate ubiquitous

formation of center-type domain and possible ferroelectric closure arrangements during polarization switching at the ferroelastic domain walls in (100) oriented rhombohedral $BiFeO_3$ thin films. Flux-closure states are associated with the symmetry breaking induced by the pre-existing ferroelastic domain walls in the system. The formation of center-type defects can be explained by the field geometry created by a PFM tip. Center-type defects were found to be stable only when formed under high localized tip-fields. The reversible changes in surface topography associated with the formation of the disclinations at the defect cores are observed. Overall, these studies suggest that formation of topological defects during localized polarization switching in multiaxial ferroelectrics is a significantly more ubiquitous phenomenon than believed previously.

METHODS

Research was carried out on two identical BFO samples. Details of sample preparation can be found elsewhere.[29] Work at UNSW was carried out with a Digital Instruments Multimode SPM with Veeco Nanoscope IIIA controller. The software used was Digital Instruments Nanoscope II version 5.12r2, and WsXM 3.0.[38] Some work was also carried out on a JEOL SPM 5400. Two SR-830 DSP lock-in amplifiers, from Stanford Research Systems, were utilized for the PFM setup. An Agilent Technologies 81150A 120 MHz pulse function arbitrary generator was used to generate pulses fed to the SPM tip. Tips used were from Nanosensors, type PPP-CONTPt-50 and were Pt/Ir coated with radii of about 7 nm, resonant frequency of 13 kHz, and force constant of 0.2 N/m. The PFM measurement at NCKU was carried out by a Veeco di-CPII SPM system, also equipped with two SR-830 DSP lock-in amplifiers. The scan-controlling and the image-analysis software were digital instruments ProScan version 1.9, and .IP (Image Processing and data analysis) version 2.1.15, respectively. The voltage pulses were applied by the PICOTEST G5100A 50 MHz function arbitrary waveform generator through the SPM tip. The conductive tips were commercial Pt/Ir-coated tips with a resonant frequency of 140 kHz and force constant of 4.5 N/m (type PPP-NCSTPt-20 Nanosensors). Some experimentation was carried out at ORNL on a commercial atomic force microscope (Asylum Research, Cypher model) equipped with NI PXI based band excitation controller to enable switching spectroscopy PFM (SS-PFM) measurements.

Acknowledgment. The research at ORNL (S.V.K., N.B.) was conducted at the Center for Nanophase Materials Sciences, which is sponsored at Oak Ridge National Laboratory by the Division of Scientific User Facilities, U.S. Department of Energy. R.K.V. and V.N. acknowledge access to the UNSW node of the Australian Microscopy & Microanalysis Research Facility (AMMRF) and ARC Discovery Project Grant DP1096669. Y.H.C. acknowledges the support of the National Science Council, R.O.C., under Contract NSC 98-2119-M-009-016. L.Q.C. is grateful for the support from DOE Basic Sciences under Grant Number DE-FG02-07ER46417. The authors acknowledge J. Scott for illuminating discussion of early work on topological defects in ferroics.

Supporting Information Available: Additional data and figures as described in the text. This material is available free of charge *via* the Internet at http://pubs.acs.org.

REFERENCES AND NOTES

1. Chaikin, P. M.; Lubensky, T. C. *Principles of Condensed Matter Physics*; Cambridge: Cambridge, U.K., 1995.
2. Wadhawan, V. K. *Introduction to Ferroic Materials*; Gordon & Breach: Amsterdam, The Netherlands, 2000.
3. Mermin, N. D. The Topological Theory of Defects in Ordered Media. *Rev. Mod. Phys.* **1979,** *51*, 591.
4. Tagantsev, A.K.; Cross, L.E.; Fousek, J. *Domains in Ferroic Crystals and Thin Films*; Springer: New York, 2010.
5. Hytch, M. J.; Dunin-Borkowski, R. E.; Scheinfein, M. R.; Moulin, J.; Duhamel, C.; Mazaleyrat, F.; Champion, Y. Vortex Flux Channeling in Magnetic Nanoparticle Chains. *Phys. Rev. Lett.* **2003,** *91*, 257207.
6. Kramer, B. *Advances in Solid State Physics*; Springer: New York, 2003; Vol. 43.
7. Tonomura, A.; Matsuda, T.; Endo, J.; Arii, T.; Mihama, K. Direct Observation of Fine Structure of Magnetic Domain Walls by Electron Holography. *Phys. Rev. Lett.* **1980,** *44*, 1430.
8. Shoenberg, D.; Wilson, A. J. C. Orientation of Ferromagnetic Domains near a Crystal Surface. *Nature* **1946,** 157.
9. Shi, J.; Tehrani, S.; Scheinfein, M. R. Geometry Dependence of Magnetization Vortices in Patterned Submicron Nife Elements. *Appl. Phys. Lett.* **2000,** *76*, 2588–2590.
10. Guslienko, K. Y.; Han, X. F.; Keavney, D. J.; Divan, R.; Bader, S. D. Magnetic Vortex Core Dynamics in Cylindrical Ferromagnetic Dots. *Phys. Rev. Lett.* **2006,** *96*, 067205.
11. Schneider, M.; Hoffmann, H.; Zweck, J. Magnetic Switching of Single Vortex Permalloy Elements. *Appl. Phys. Lett.* **2001,** *79*, 3113–3115.
12. Jungk, T.; Hoffmann, A.; Fiebig, M.; Soergel, E. Electrostatic Topology of Ferroelectric Domains in $YMnO_3$. *Appl. Phys. Lett.* **2010,** *97*, 012904–012903.
13. Fiebig, M.; Lottermoser, T.; Frohlich, D.; Goltsev, A. V.; Pisarev, R. V. Observation of Coupled Magnetic and Electric Domains. *Nature* **2002,** *419*, 818–820.
14. Šafránková, M.; Fousek, J.; KiŽaev, S. A. Domains in Ferroelectric $YMnO_3$. *Czech. J. Phys.* **1967,** *17*, 559–560.
15. Gonzalo, J. A.; Jiménez, B. *Ferroelectricity: The Fundamentals Collection*; Wiley-VCH: New York, 2005; Vol. 10.
16. Gorbatsevich, A. A.; Kopaev, Y. V. Toroidal Order in Crystals. *Ferroelectrics* **1994,** *161*, 321–334.
17. Naumov, I. I.; Bellaiche, L.; Fu, H. Unusual Phase Transitions in Ferroelectric Nanodisks and Nanorods. *Nature* **2004,** *432*, 737–740.
18. Prosandeev, S.; Bellaiche, L. Properties of Ferroelectric Nanodots Embedded in a Polarizable Medium: Atomistic Simulations. *Phys. Rev. Lett.* **2006,** *97*, 167601.
19. Prosandeev, S.; Bellaiche, L. Characteristics and Signatures of Dipole Vortices in Ferroelectric Nanodots: First-Principles-Based Simulations and Analytical Expressions. *Phys. Rev. B* **2007,** *75*, 094102.
20. Prosandeev, S.; Ponomareva, I.; Kornev, I.; Bellaiche, L. Control of Vortices by Homogeneous Fields in Asymmetric Ferroelectric and Ferromagnetic Rings. *Phys. Rev. Lett.* **2008,** *100*, 047201.
21. Lahoche, L.; Luk'yanchuk, I.; Pascoli, G. Stability of Vortex Phases in Ferroelectric Easy-Plane Nano-Cylinders. International Symposium on Integrated Ferroelectrics ISIF, 2007; Taylor and Francis: London, 2008; Vol. 99, Number 1, pp 60−66.
22. Sene, A.; Baudry, L.; Luk'yanchuk, I. A.; Lahoche, L. Field-Induced Vortices in Weakly Anisotropic Ferroelectrics *arXiv* [Online], 2009. http://www.citebase.org/abstract?id=oai:arXiv.org:0909.1757.
23. Gruverman, A.; Wu, D.; Fan, H. J.; Vrejoiu, I.; Alexe, M.; Harrison, R. J.; Scott, J. F. Vortex Ferroelectric Domains. *J. Phys.: Condens. Matter* **2008,** *20*, 342201.
24. Rodriguez, B. J.; Gao, X. S.; Liu, L. F.; Lee, W.; Naumov, I. I.; Bratkovsky, A. M.; Hesse, D.; Alexe, M. Vortex Polarization States in Nanoscale Ferroelectric Arrays. *Nano Lett.* **2009,** *9*, 1127–1131.

25. Schilling, A.; Byrne, D.; Catalan, G.; Webber, K. G.; Geneko, Y. A.; Wu, G. S.; Scott, J. F.; Gregg, J. M. Domains in Ferroelectric Nanodots. *Nano Lett.* **2009,** *9*, 3359–3364.
26. McGilly, L. J.; Schilling, A.; Gregg, J. M. Domain Bundle Boundaries in Single Crystal $BaTiO_3$ Lamellae: Searching for Naturally Forming Dipole Flux-Closure/Quadrupole Chains. *Nano Lett.* **2010,** *10*, 4200–4205.
27. Balke, N; Choudhury, S; Jesse, S; Huijben, M; Chu, Y. H.; Baddorf, A. P.; Chen, L. Q.; Ramesh, R; Kalinin, S. V. Deterministic Control of Ferroelastic Switching in Multiferroic Materials. *Nat Nano* **2009,** *4*, 868–875.
28. Brown, M. E.; Hollingsworth, M. D. Stress-Induced Domain Reorientation in Urea Inclusion Compounds. *Nature* **1995,** *376*, 323–327.
29. Chu, Y.-H.; Zhan, Q.; Martin, L. W.; Cruz, M. P.; Yang, P.-L.; Pabst, G. W.; Zavaliche, F.; Zhang, S.-Y. Y. J.-X.; Chen, L.-Q.; Schlom, D. G.; *et al.* Nanoscale Domain Control in Multiferroic $BiFeO_3$ Thin Films. *Adv. Mater.* **2006,** *18*, 2307–2311.
30. Wicks, S.; Seal, K.; Jesse, S.; Anbusathaiah, V.; Leach, S.; Edwin Garcia, R.; Kalinin, S. V.; Nagarajan, V. Collective Dynamics in Nanostructured Polycrystalline Ferroelectric Thin Films Using Local Time-Resolved Measurements and Switching Spectroscopy. *Acta Mater.* **2010,** *58*, 67–75.
31. Ivry, Y.; Chu, D. P.; Scott, J. F.; Durkan, C. Flux Closure Vortexlike Domain Structures in Ferroelectric Thin Films. *Phys. Rev. Lett.* **2010,** *104*, 207602.
32. Chen, L.-Q. Phase-Field Models for Microstructure Evolution. *Ann. Rev. Mater. Res.* **2003,** *32*, 113–140.
33. Li, Y. L.; Hu, S. Y.; Liu, Z. K.; Chen, L. Q. Effect of Substrate Constraint on the Stability and Evolution of Ferroelectric Domain Structures in Thin Films. *Acta Mater.* **2002,** *50*, 395–411.
34. Li, Y. L.; Hu, S. Y.; Liu, Z. K.; Chen, L. Q. Effect of Electrical Boundary Conditions on Ferroelectric Domain Structures in Thin Films. *Appl. Phys. Lett.* **2002,** *81*, 427–429.
35. Zhang, J. X.; Li, Y. L.; Wang, Y.; Liu, Z. K.; Chen, L. Q.; Chu, Y. H.; Zavaliche, F.; Ramesh, R. Effect of Substrate-Induced Strains on the Spontaneous Polarization of Epitaxial $BiFeO_3$ Thin Films. *J. Appl. Phys.* **2007,** *101*, 114105–114106.
36. Zhang, J. X.; Li, Y. L.; Choudhury, S.; Chen, L. Q.; Chu, Y. H.; Zavaliche, F.; Cruz, M. P.; Ramesh, R.; Jia, Q. X. Computer Simulation of Ferroelectric Domain Structures in Epitaxial $BiFeO_3$ Thin Films. *J. Appl. Phys.* **2008,** *103*, 094111–094116.
37. Anbusathaiah, V.; Jesse, S.; Arredondo, M. A.; Kartawidjaja, F. C.; Ovchinnikov, O. S.; Wang, J.; Kalinin, S. V.; Nagarajan, V. Ferroelastic Domain Wall Dynamics in Ferroelectric Bilayers. *Acta Mater.* **2010,** *58*, 5316–5325.
38. Horcas, I.; Fernandez, R.; Gomez-Rodriguez, J. M.; Colchero, J.; Gomez-Herrero, J.; Baro, A. M. WSXM: A Software for Scanning Probe Microscopy and a Tool for Nanotechnology. *Rev. Sci. Instrum.* **2007,** *78*, 013705–013708.